Molecular Dynamics Simulation Study of Ethylene Glycol, Ethylenediamine, and 2-Aminoethanol. 1. The Local Structure in Pure Liquids

A. V. Gubskaya and P. G. Kusalik*

Department of Chemistry, Dalhousie University, Halifax, Nova Scotia, B3H 4J3, Canada

Received: March 10, 2004; In Final Form: June 17, 2004

This paper describes a comparative molecular dynamics (MD) simulation study of the local structure of pure liquid ethylene glycol (EG), ethylenediamine (ED), and 2-aminoethanol (AE), which are three well-known representatives of 1,2-disubstituted ethanes. As an essential component of this investigation, 12 molecular models were constructed and their gas-phase characteristics were determined. The results obtained for the molecular geometries were compared with the most reliable experimental estimates, to test different force fields and molecular representations. Liquid-phase simulations were then performed on the more successful (OPLS-based) models. The heats of vaporization and self-diffusion coefficients were used as criteria for the final selection of molecular models to be used in our subsequent detailed structural analysis. The dihedral angle distributions were calculated and relative populations of rotational isomers, with respect to the central dihedral angle, were determined. It was confirmed that, for pure liquid EG and AE, the *gauche* conformation accounts for the major population of isomers, whereas ED exhibits a significant population of *trans* conformers. The analysis of radial distribution functions (RDFs), in conjunction with calculated numbers of nearest neighbors around the O and N atoms of the main functional groups, provided some structural insights into the hydrogen-bonding pattern of the systems studied. The number of strongly hydrogen-bonded neighboring groups was determined, and their possible positions were located by means of spatial distribution functions (SDFs). The possibility of three- and four-membered nearest-neighbor arrangements (comprised of two strong and, at most, two weak hydrogen bonds) found around O and N atoms leads to the conclusion that, in the pure liquids of EG, ED, and AE, the generalized hydrogen-bonding pattern can be described as a three-dimensional, branched network.

1. Introduction

1,2-Disubstituted ethanes comprise the group of saturated molecules with the general formula XCH_2CH_2Y, where the functional groups X and Y are, for example, F, Cl, NH_2, and OH.[1] In the present study, the widely used representatives of this group—$(CH_2NH_2)_2$ (ethylenediamine), $NH_2(CH_2)_2OH$ (2-aminoethanol), and $(CH_2OH)_2$ (ethylene glycol)—will be considered. These molecules contain amino and/or hydroxyl groups, each of which can simultaneously act as donors and acceptors of hydrogen bonds.

Ethylenediamine, 2-aminoethanol, and ethylene glycol (hereafter referenced as ED, AE, and EG, respectively) have a variety of applications in chemistry and the chemical industry.[2−4] With their carbon backbone and the presence of polar groups participating in both intramolecular and intermolecular hydrogen-bond interactions, these compounds can also serve as small prototypical systems in developing parameters for macromolecular modeling. For example, a realistic representation of the intramolecular hydrogen-bonding patterns of vicinal hydroxyl groups in EG is crucial to the modeling of sugars and their polymers,[5] as well as the side chains of serine, threonine, tyrosine, and several less-common amino acids.[6] Although EG is a small organic molecule, it may be considered as a water analogue. It has one of the lowest ratios among alcohols of weakly polar methylene (or methyl) groups to polar hydroxyl groups, which means that its properties will be strongly influenced by hydrogen-bonding interactions. However, in contrast to water, EG will exhibit a competition between intermolecular and intramolecular interactions (hydrogen bonds), which is a common distinctive feature shared by pure molecular liquids of EG, ED, and AE.

The study of small functionalized organic molecules is a typical first step in the modeling of larger molecular systems. Among the variety of possible representatives of hydrogen-bonded liquids composed of "small organic molecules", methanol and methylamine are the most widely studied.[6−15] The pattern of hydrogen bonding in methanol and methanol-like systems seems to be very different from that found in water. It has been shown experimentally[7] and theoretically[9,11] that, instead of forming tetrahedral networks in liquid methanol each molecule engages in approximately two hydrogen bonds, which is consistent with a chainlike structure. It seems that these hydrogen-bonded chains prefer a local parallel arrangement that is similar to that observed in the solid state.[8] In contrast to methanol, within liquid methylamine molecules prefer arrangements with a few amino groups clustered together in small compact ring or ring-like structures.[15] Given these findings, it is particularly interesting to observe the local structure in liquid systems with both alcohol and amino groups present (e.g., AE).

1,2-Disubstituted ethanes (XCH_2CH_2Y) possess internal rotation, which results in the three possible rotameric dihedral angles: one about the C−C bond and one about each of the C−X and C−Y bonds. Ten unique possible conformers can be

* Author to whom correspondence should be addressed. Telephone: (902) 494-3627. Fax: (902) 494-1310. E-mail address: Peter.Kusalik@dal.ca.

10.1021/jp0489222 CCC: $27.50
Published on Web 08/11/2004

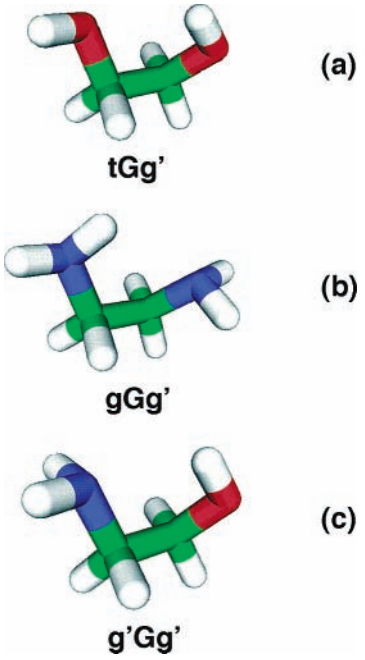

Figure 1. Molecular structures of the most-stable conformers in the gas phase: (a) ethylene glycol (EG), (b) ethylenediamine (ED), and (c) 2-aminoethanol (AE). The green, red, and blue components represent C, O, and N atoms, respectively.

generated for ED and EG and fourteen for AE. The notation for identifying rotational isomers of the XCH_2CH_2Y is given in refs 1 and 16.

In the gas phase, the conventional conformational analysis of EG, ED, and AE, which includes determination of the most stable unique conformers and their relative stabilities, has been performed by means of *ab initio* techniques, mainly at the HF and MP2 levels of theory.[1,2,5,17−27] There have also been some interesting attempts to evaluate the rotational flexibility of these molecules through examination of the heights of potential barriers for the most important conformational interconversions.[18,26,28,29] It has been clearly shown that the most stable conformers of these three molecules are tGg′, gGg′, and g′Gg′ (see Figure 1) for EG, ED, and AE, respectively.[18] In addition, Chang et al.[18] examined the relative contributions from hydrogen-bonded interactions and the *gauche effect* to the stability of the lowest-energy conformers for the compounds of interest. The final conclusion of their conformational analysis was that intramolecular hydrogen bonding plays a major role in the stabilization of *gauche* conformers in comparison with *trans* conformers. The strength of the hydrogen bond decreases in the order AE $\cong$ EG > ED; thus, it would be expected that, in the condensed phase, this trend will also be preserved, i.e., AE should behave conformationally similarly to EG, whereas ED would behave differently.[18]

A limited number of theoretical studies of liquid 1,2-disubstituted ethanes have been published within the past decade.[22,30−35] EG has been the most extensively investigated, although it is perhaps somewhat surprising that no computational studies of liquid ED can be found in the available literature. Padro, Saiz, and Guardia[31] performed a series of MD simulations to investigate hydrogen bonding in liquid methanol, ethanol, EG, and glycerol at 298 K. It was found that EG seemed to show three-dimensional hydrogen-bonding patterns, although these were not well-characterized.[31] The same group of authors[30] later examined the structure of liquid EG at room temperature by performing MD simulation studies for four different force fields, namely, J,[6] JMOD,[30] WP,[32] and HTN.[33] It was observed that the structure seems to be dominated by a three-dimensional network of hydrogen-bonded molecules with a mean number of hydrogen bonds per molecule slightly lower than four.[31] Interestingly, the structural results obtained were similar for each model and seemed to be independent of the mean conformation of the molecule. In contrast, the data obtained for the dynamics indicated that the four models give quite different results, suggesting significant differences in the local molecular environment. The authors found good agreement for the self-diffusion coefficients between the OPLS-based models (7.4×10^{-7} and 11.7×10^{-7} cm^2/s for J and JMOD, respectively) and the experimental value of 9.0×10^{-7} cm^2/s.[36]

The number of theoretical studies of liquid AE is small, and these have not focused in detail on its thermodynamic and structural behavior. In 1996, Button et al.[34] used MD simulations to study hydrogen bonding in liquid AE. The authors used a force field that was a combination of those reported for alcohols and amines.[34] The results were not compared to experimental data, and the major conclusion of Button et al.[34] was that "different behavior was observed for the alcohol and amine functional groups". Later, Alejandre et al.[35] developed a special force field for AE as a precursor of a more general modeling potential for simulations of alkanolamines and their aqueous solutions. The proposed force field satisfactorily reproduces the experimental dipole moment, the liquid-vapor coexistence, and the surface tension of AE.[35]

The present work is a comparative MD simulation study of the local structure in liquid EG, ED, and AE. Several models for each of these molecules are considered. Comparison of gas-phase geometries and of liquid-phase dynamic and thermodynamic properties are then used to identify the most successful models to be utilized in our subsequent detailed structural analysis. Elucidation of the local structure and the hydrogen-bonding patterns in these systems is performed by means of both radial and spatial distribution functions (RDFs and SPFs, respectively). We find that, for pure liquid EG and AE, the majority of the molecules are in the *gauche* conformation (with respect to the central dihedral angle), whereas, for ED, the population of *trans* conformers is dominant. Our analysis of the three-dimensional local molecular environments reveals rather complex structural patterns arising from the internal rotational flexibility of these molecules. Nevertheless, strong association between appropriate functional groups is identified where three- and four-membered nearest-neighbor arrangements comprised of two strong and, at most, two weak hydrogen bonds are apparent around hydroxyl and amino groups. This leads to the conclusion that, in all these liquids, the generalized hydrogen-bonding structure can be characterized as being a three-dimensional, branched network.

This article is organized as it follows. In Section II, the potential models and computational methodology used are described in detail. The results of simulations performed on isolated molecules, as well as for pure liquid EG, ED, and AE are presented and discussed in a comparative manner in the Section III. Finally, Section IV is devoted to our concluding remarks. In a following companion paper the same methodological approach and molecular models are used to investigate the local structure of EG, ED and AE in an aqueous surrounding.[37]

2. Methodological Details

2.1. Molecular and Potential Models. In the present study, each molecule was first modeled using a united atom ap-

proximation[38] in which the H atoms of the methylene (CH_2) groups were not explicitly considered but taken into account implicitly in the parameters. In this approximation, the EG molecule consisted of six interaction sites, the AE molecule of seven interaction sites, and the ED molecule of eight interaction sites. The CH_2 groups were considered as single interaction sites, with their centers located at the position of the C atoms. All bond lengths were kept fixed by means of the SHAKE algorithm[39] during essentially all of the present simulations. However, for the purpose of comparison, two additional models were constructed: an all-atom model of EG with fixed bond lengths (represented by 10 interaction sites) and a fully flexible united atom model of AE. Both of these models were studied in the gas phase as well as in the liquid state.

Three AMBER/OPLS-based force fields by Jorgensen and co-workers[6,40,41] were considered in the present study. The generalizations of the OPLS model proposed for simulations of liquid alcohols[6] and amines[40] were used to describe intramolecular and intermolecular interactions in EG and ED. For AE bond lengths, bond angles and nonbonded parameters specifically for hydroxyl and amino groups were taken from refs 6 and 40, respectively. MM3 type potentials[6,40,42] were used for torsional angles of principal ED, EG, and AE models. The all-atom characteristics for the CH_2 groups from ref 41, in conjunction with parameters for hydroxyl groups, and the torsion potential from ref 6 were used in the all-atom molecular model of EG. In addition, two auxiliary force fields, CHARMM and that proposed by Alejandre et al.,[35] were applied to AE for the sake of comparison of potential models. For all models, 1−4 nonbonded interactions (for the sites separated by exactly three covalent bonds) were included in the calculations. For selected models, 1−4 electrostatic and Lennard-Jones (LJ) interactions were scaled by factors of 1/1.2 (from ref 43) and 1/8 (from refs 44 and 45), respectively.

2.2. Simulation Specifications. A truncated octahedron simulation cell with corresponding periodic boundary conditions were utilized in all our simulations. The cross terms of the LJ parameters were calculated using simple Lorentz−Berthelot combination rules and the optimized Ewald method was used to treat the Coulombic interactions.[46,47] All calculations were carried out at room temperature (298 K) and experimental densities of 0.8990,[48] 1.1003,[49] and 1.0118 g/cm^3,[50] respectively, for ED, EG, and AE in the NVT ensemble. The temperature was maintained by a Nosé−Hoover thermostat[51,52] with a relaxation time of 300 fs. The main simulation software was the parallel scalable simulation package M.DynaMix.[47] Molecular geometries were optimized by means of the GAUSSIAN 98 program.[53] Visualization of current configurations and of SDFs has been performed using XMol and gOpenMol software.[54]

To model gas-phase conditions, single molecule calculations of a total duration of 25 ps with a time step of 1 fs were performed. Gas-phase geometries (conformations) of ED, AE, and EG have been used as the starting geometries for all liquid-phase simulations. Liquid systems consisting of 256 molecules per simulation cell were simulated for 300 ps (with averages collected after 100 ps of equilibration). We have found that, to achieve convergence of configurational energies, a trajectory of 50−100 ps is required, whereas the stabilization of self-diffusion coefficients and a sampling of major conformations can require a total trajectory length of 300−400 ps, in accord with the results presented in refs 15, 30, and 35. Unfortunately, a complete sampling of all dihedral angles, assuming three dihedral angles per molecule, would require significantly longer (i.e., multiple nanoseconds) runs with standard simulation techniques.

TABLE 1: Basic Gas-Phase Simulation Results for Different Models of 2-Aminoethanol (AE) at 298 K

	AEop	AEeq	AEcmb	AEtst	AEchm
average energy (kJ/mol)					
$\langle U_a \rangle$	4.78	4.34	2.40	1.71	19.11
$\langle U_d \rangle$	3.14	2.94	7.90	−3.14	1.20
$\langle U_Q \rangle$	60.59	60.86	72.97	165.05	128.36
$\langle U_{LJ} \rangle$	3.04	2.87	0.94	0.14	14.30
$\langle U \rangle$[a]	71.55	71.01	84.21	163.76	162.98
average angle (deg)					
NCC	108.1	109.1	111.2	118.7	124.1
OCC	107.6	105.9	107.9	108.9	119.5
HNC	110.5	109.0	109.3	110.5	110.0
HOC	102.2	102.9	104.7	105.7	104.5
dihedral angle (deg)					
NCCO	−41.5	38.3	45.8	−83.4	0.1
HOCC	22.7	−16.4	−33.7	46.5	−47.0
HNCC	−179.7	−171.2	−173.8	179.8	−168.2
conformation	**gG′g′**	**c′Gg′**	**g′Gg′**	**gG′g**	**g′Cg′**

[a] The largest error associated with the total configurational energies is ∼0.1 kJ/mol.

The total average configurational energy, $\langle U \rangle$, was obtained as a part of the standard output of the M.DynaMix program. This quantity can be directly compared to the experimentally determined heats of vaporization. The molar heat of vaporization was calculated in the usual way (see ref 44).

In publications devoted to the development of model potentials for relatively small molecules,[6,40,44,55] it has become common practice to use the experimentally determined heat of vaporization as a principal criterion for evaluating the quality of the parametrization. It is unfortunate that such a comparison seems to have been abandoned in a majority of publications on 1,2-disubstituted ethanes in the liquid state, independent of the kind of force field (conventional or newly developed) that was used.[30,31,34,35] In this work, the computed heats of vaporization are compared to available experimental data to help select the best model representation for pure liquids of AE, ED and EG (as well as their aqueous solutions[37]).

3. Results and Discussion

3.1. Gas-Phase Systems. In the present study, gas-phase (single-molecule) simulations were performed as a first stage in the investigation of structural behavior in liquid systems. It is well-known that, in liquid phase simulations, the quality of the final results is strongly dependent on the adequacy of the chosen force field and modeling conditions.[30] In this context, gas-phase simulations represent an attractive choice for preliminary testing of potential and molecular models in particular, because they allow for direct comparison with the experimental literature.

Gas-phase simulation results for thermodynamic and structural properties (i.e., the average bond angle and dihedral angle energies ($\langle U_a \rangle$ and $\langle U_d \rangle$, respectively), the average Coulombic and LJ energies ($\langle U_Q \rangle$ and $\langle U_{LJ} \rangle$, respectively), the total average configurational energy ($\langle U \rangle$), and values of the dihedral angles) for different models of AE, ED, and EG at 298 K are given in Tables 1 and 2. In accord with experimental and previous theoretical findings (see, for example, ref 18), the lowest energy conformations in the gas phase are g′Gg′ (or gG′g), g′Gt, and gGg′ for AE, EG, and ED, respectively. To allow for comparison with these results, the conformational arrangements for each model are also included in Tables 1 and 2.

TABLE 2: Basic Gas-Phase Simulation Results for Different Models of Ethylene Glycol (EG) and Ethylenediamine (ED) at 298 K

	EGex1	EGex2	EGeq	EGaa	EDex	EDop
average energy (kJ/mol)						
$\langle U_a \rangle$	1.14	1.52	1.17	18.97	2.54	2.49
$\langle U_d \rangle$	9.00	10.22	9.20	10.92	−9.07	−9.27
$\langle U_Q \rangle$	82.31	77.43	82.46	−196.63	57.08	58.59
$\langle U_{LJ} \rangle$	0.49	0.54	0.36	154.37	1.10	0.98
$\langle U \rangle$[a]	92.95	89.72	93.20	−12.37	51.65	52.78
average angle (deg)						
OCC or NCC	109.7	108.9	109.8	104.7	111.4	112.2
HOC or HNC	107.8	101.2	108.3	109.7	106.2	106.2
HOC or HNC	104.7	104.8	105.2	103.8	109.0	110.3
dihedral angle (deg)						
OCCO or NCCN	58.5	57.9	57.9	48.8	52.2	51.2
HOCC or HNCC	−52.0	−51.4	−55.6	−36.4	−40.8	−46.5
HOCC or HNCC	178.8	−168.6	−173.3	173.9	−174.4	−173.2
conformation	**g′Gt**	**g′Gt**	**g′Gt**	**g′Gt**	**gGg′**	**gGg′**

[a] The largest error associated with total configurational energies is ∼0.02 kJ/mol.

The applicability of different force fields, in particular, Jorgensen's AMBER/OPLS-based,[40,41] a "combined" model potential,[6,40] CHARMM,[56,57] and the special force field by Alejandre et al.[35] have been tested with the corresponding equilibrium geometries in single molecule simulations of AE (denoted as the AEeq, AEcmb, AEchm, and AEtst models, respectively, in Table 1). Comparison of data from Table 1 with experimental geometric parameters[24,58−60] clearly indicates that both the AEeq and AEtst models give very good performance, in terms of reproducing the corresponding gas-phase geometry, whereas the CHARMM potential generates noticeable distortion of the NCC and OCC bond angles, and, as a result, exhibits an eclipsed conformation, with respect to the central torsion angle. AE was also used to examine the possible influence of molecular model representation (not shown in Table 1). No noticeable difference in the average molecular geometry was observed between constrained and fully flexible molecular models; however, there was a small (∼1 kJ/mol) change in the average intramolecular configurational energy.

United and all-atom AMBER/OPLS molecular representations were tested on two models of EG (in Table 2, EGeq and EGaa, respectively). Only a very subtle shift in the average geometrical parameters for both these models was noted, while the configurational energy contributions were significantly rearranged. The rearrangement mainly involves the energy contributions from bond angle and intramolecular interaction (both LJ and electrostatic) terms. The latter fact can be appropriately evaluated when gas-phase configurational energies are compared with corresponding values from liquid-phase simulations.

In the testing of the different model potentials, the most important observation is the reproduction of the lowest-energy conformation for each compound of interest. There are two complementary ways to clarify this issue. In the first, the most stable conformation (obtained experimentally or by *ab initio* methods) is used as an initial input for these classical vacuum simulations and, in the case of an appropriate choice of the force field, the final conformation is expected to be essentially unchanged within acceptable error. When the most successful force field has been identified, the simulation run is then repeated, starting from an arbitrarily chosen conformational arrangement, to prove the ability of the potential in again generating the lowest-energy conformer. The results of the application of these procedures are given in Tables 1 and 2. Relying on values for the dihedral angles, all potentials (with the exception of CHARMM) reproduce the initial arrangement quite well, with slight variations. In the case when the special AE force field was used (AEtst), the optical isomer produced is the most stable conformation of AE known, whereas, for the AMBER/OPLS-based models (AEop and AEeq), the value for the HOCC angle was definitely too low (in comparison with the conventional value for a *gauche* arrangement). The model AEcmb was designed to test a "combined" torsion potential where the Fourier coefficients for the NCCO and HOCC torsion angles were taken from a force field for liquid alcohols[6] and those for the HNCC angle came from a model potential for amines.[40] At the present level of analysis, AEcmb seems to provide a good representation of an AE molecule in the gas phase. In particular, it is the only model among all those considered for AE that exactly reproduces its most stable conformation (g′Gg′) with a reasonable average value (55°) for the NCCO torsion angle.

An analysis of the gas-phase simulation results obtained from models developed using different geometric parameters also revealed some interesting trends. Two groups of geometry-dependent models were considered: those based exclusively on experimental parameters such as EGex1 (gas-phase data by Caminatti and Corbelli[59]), EGex2 (liquid-phase structure by Buckley and Giguere[60]), EDex and AEex (gas-phase measurements by Marstokk and Mollendal[58] and Penn and Curl,[24] respectively), as well as models based on optimized structures such as AEop and EDop. In all cases, the bond lengths of these model molecules were treated as being rigid, using a united atom representation and the AMBER/OPLS force field. The final structural characteristics for the EGex1, EGex2, and EDex models correlate well with the original experimental data.[58−60] Both the EGex1 and EGex2 models predict very similar geometries, as well as thermodynamic properties (see Table 2). Entirely consistent behavior is observed between the characteristics from EDex and EDop. All the models presented in Table 2 reproduce the most stable conformations of EG and ED quite well, indicating a consistently adequate combination of the force field and model geometry.

In contrast to EG and ED, the experimental-geometry-based model for AE (not shown in Table 1) exhibited a rather distorted structure. Utilization of the geometry following optimization of this experimental structure with a modest basis set (6-31+G-(d)) at the MP2 level of theory significantly improves this situation; final geometric parameters for AEop were in good agreement with data obtained from the tests for AEeq and AEcmb. Overall, bond and dihedral angles for both AMBER/OPLS-based models seem to be smaller, in comparison with those for AEcmb, as is apparent in the magnitudes of corre-

TABLE 3: Coulombic and Lennard-Jones (LJ) Contributions to the Total Configurational Energy and Heats of Vaporization of Liquid Ethylene Glycol (EG), Ethylenediamine (ED), and 2-Aminoethanol (EA) at 298 K

	EGex2	EGaa	EDex	AEcmb	AEtst
intramolecular energy (kJ/mol)					
$\langle U_Q \rangle$	88.17	−194.30	61.29	81.11	169.49
$\langle U_{LJ} \rangle$	0.89	161.65	1.68	0.87	−0.16
intermolecular energy (kJ/mol)					
$\langle U_Q \rangle$	−60.38	−34.35	−35.54	−48.16	−36.80
$\langle U_{LJ} \rangle$	−8.65	−16.15	−15.98	−13.62	−16.37
total energy, $\langle U \rangle$ (kJ/mol)	29.21 ± 0.04	−60.79 ± 0.02	19.32 ± 0.03	34.67 ± 0.03	128.36 ± 0.03
heat of vaporization, ΔH_{vap} (kJ/mol)					
experiment	63.04 ± 0.07	50.92 ± 0.03	34.83 ± 0.05	52.04 ± 0.05	37.90 ± 0.03
literature values	57.0−65.6[a]	57.0−65.6[a]	44.98[b]	55.33[c]	55.33[c]

[a] Data taken from refs 61−63. [b] Data taken from ref 62. [c] A correction of 5.5 kJ/mol has been added to the value of 49.83 kJ/mol (from ref 66).

sponding energy contributions. However, in the absence of reliable experimental data, it is difficult to make a definite conclusion about the relative quality of the calculated geometries for an isolated molecule of AE.

3.2. Liquid-Phase Simulations. Our analysis of gas-phase simulations results has shown that the information obtained is necessary but not sufficient for a critical assessment of the quality of the molecular models and interaction potentials. On the basis of gas-phase results, only two models, namely AEchm (giving the wrong conformation, with respect to the central dihedral angle) and EDop (giving essentially the same results as the EDex model), were excluded from calculations of liquid AE, ED, and EG. Therefore, there was still a need to impose additional criteria, which would allow the elimination of the least successful models from the present set.

3.2.1. Selection of Liquid-Phase Models. The criteria chosen for preliminary selection of liquid-phase models were the liquid density and heats of vaporization. The density of all models (at a pressure of 1 atm) was examined. For example, the density of liquid ED (0.9443 g/cm^3) obtained from a constant-pressure MD run for the EDex model, which is a typical representative for all AMBER/OPLS-based models, was in reasonable agreement (within ∼5%) with the experimental value of 0.8990 g/cm^3 at 1 atm,[48] confirming the applicability of the AMBER/OPLS force field to the compounds of interest.

The different contributions to the total configurational energies for the selected liquid-phase models are given in Table 3, as well as the calculated and experimentally determined heats of vaporization (ΔH_{vap}). Special note should be made with respect to the experimental values given in Table 3. In particular, in the contemporary scientific literature, one can find at least three different values for ΔH_{vap} of EG at 298 K, namely 57.07,[61] 58.71,[62] and 65.6 kJ/mol.[63] The latter value is the most recent estimate deduced from direct calorimetric measurements of alkanediols.[63−65] For AE, the only experimental value of ΔH_{vap} was measured at its boiling temperature (T_b = 444 K),[66] making a direct comparison with data obtained at 298 K difficult. We have estimated the temperature-dependent correction to the experimental ΔH_{vap} value (5.5 kJ/mol) by considering an appropriate thermodynamic cycle based on data for heat capacities given in ref 66. From our assessment, the corrected value of the experimental ΔH_{vap} value for AE at 298 K is 55.33 kJ/mol.

Table 3 shows that the heat of vaporization calculated for the AEtst model is in rather poor agreement with the experimental value, whereas AEcmb gives excellent performance. It can also be noted that there are significant discrepancies between the experimental and calculated results for the EDex and EGaa models. The EDex model has the lowest-magnitude ΔH_{vap} value among the all models presented in Table 3.

An analysis focusing mainly on values for the heat of vaporization and other key properties (i.e., self-diffusion coefficients) allowed for highlighting and elimination of some of the least successful models for each compound. In particular, the EGaa (with its rather large error in ΔH_{vap}) and EGex2 (with a similar magnitude error in ΔH_{vap} as for the EGex1 model, but with a self-diffusion coefficient of ∼20% of the experimental value) models were removed from further consideration. Hence, at this stage, only one model (EGex1) remained for EG; for ED, the EDex model was chosen (despite its large error in ΔH_{vap}), because no obviously better alternative was available. For AE, two models were retained for further consideration: AEcmb, which has the superior thermodynamic and dynamic properties, and AEtst as the test representative of a specifically designed model potential. Therefore, at this stage of the present analysis, EGex1, EDex, and AEcmb can be identified as our primary models for further examination.

In force-field development, one of the ways for possibly improving the agreement between calculated and experimental data is by adjusting parameters in the Coulomb and LJ energy terms for the so-called 1−4 nonbonded interactions.[43,45] This can be achieved by exploring the appropriate scaling factors. All the data reported in Tables 1, 2, and 3 (with the exception of the AEtst model) were obtained with the standard scaling factors of 0.833 and 0.125 for the electrostatic[30,43] and LJ[45] nonbonded interactions, respectively. However, we have determined that, for 1,2-disubstituted ethanes, the heat of vaporization is not the only parameter, which is sensitive to the scaling applied. The major population of rotational isomers and the self-diffusion coefficient, D, in liquid-phase systems are rather sensitive to the values used to scale the nonbonded parameters. In this work, we varied and tested several different pairs of values for 1−4 scaling. The results obtained confirmed that only two possibilities—namely, the previously derived pair of 0.125 and 0.833,[43,45] as well as the pair of 1 and 1 (i.e., no scaling used), for van der Waals and electrostatic terms, respectively—seem to be among the most promising possibilities.

3.2.2. Dihedral Angle Distributions. The conformational characteristics—in particular, dihedral angle distributions—were examined for the EGex1, EDex, and AEcmb (henceforth referenced as EG, ED, and AE, respectively) models, as well as the AEtst model, for testing purposes. For each of the EG, ED, and AE models, two separate liquid-phase simulation runs were performed with the standard scale factors (0.125 for LJ and 0.833 for electrostatic terms) and no scaling (1 and 1, respectively) applied. Only the latter scaling scheme[35] was used for the AEtst model. Although all three torsional angles were monitored during our simulations, in the analysis below, it is sufficient to focus only on the rotation around the central dihedral angles. For each molecule, this torsional angle is

TABLE 4: Conformational Characteristics of Pure Liquid Ethylene Glycol (EG), Ethylenediamine (ED), and 2-Aminoethanol (EA) at 298 K

	EGex1			EDex					AEcmb	AEtst	
scale factors	0.125; 0.833		1; 1	0.125; 0.833		1; 1			0.125; 0.833	1; 1	
conformation	G′	G	T	G′	G	G′	G	T	G	G	T
(%)	0.9	99.1	100	16.6	83.4	16.2	19.6	64.2	100	20	80
dihedral angle (deg)[a]	−42.5	57.5	182.5	−52.5	52.5	−67.5	67.5	182.5	−62.5	77.5	177.5

[a] All values for dihedral angles correspond to the maximum probability of dihedral angle distributions.

TABLE 5: Dependence on 1−4 Interaction Parameters of Key Results for Liquid Ethylene Glycol (EG), Ethylenediamine (ED), and 2-Aminoethanol (AE) at 298 K

	EG		ED		AE	
scale factors	0.125; 0.833	1; 1	0.125; 0.833	1; 1	0.125; 0.833	1; 1
conformation						
experiment	G	T	G	G+T	G	G
literature value	G[a]		G+T/T[b]		G[c]	
H_{vap} (kJ/mol)						
experiment	53.37 ± 0.04	67.40 ± 0.08	34.83 ± 0.05	40.01 ± 0.03	52.04 ± 0.05	52.13 ± 0.01
literature value	57.0−65.6[d]		44.98[e]		55.33[f]	
D ($\times 10^{-5}$ cm^2/s)						
experiment	0.08	0.012	1.16	1.0	0.2	0.08
literature value	0.09[g]		0.98[h]			

[a] Data taken from refs 67 and 68. [b] Data taken from ref 2. [c] Data taken from ref 69. [d] Data taken from refs 61−63. [e] Data taken from ref 62. [f] A correction of 5.5 kJ/mol has been added to the value of 49.83 kJ/mol (from ref 66). [g] Data taken from ref 36. [h] Data taken from ref 70.

characterized by the highest (∼20−30 kJ/mol) energy barrier and is responsible for determining the presence (formation) of an intramolecular hydrogen bond. An additional comment should also be made, with regard to torsional angle sampling. We have found that the averaging of torsional angles seems to be an extremely slow process and complete averages would require very long simulation runs. Our simulations are of sufficient duration that the majority of the most stable (or key) conformations—in particular, those with respect to the central dihedral angle—were clearly identified and satisfactorily sampled.

Parameters that characterize distributions with respect to the central dihedral angle for all models considered are shown in Table 4. It can be seen that, when 1−4 scaling is used for EG, the major population of rotamers (99%) is in the *gauche* conformation, with respect to the OCCO dihedral angle with the maximum probability of the distribution centered at 57.5°. In contrast, for the EG model simulated without scaling of the 1−4 interactions (see Table 4), all molecules are in the *trans* conformation, with respect to the central dihedral angle of 182.5°.

The ED model simulated with 1−4 scaling (see also Table 4) has two peaks in the NCCN dihedral angle distribution, located in the G (83.4% of conformers) and G′ (16.6% of conformers) regions. A trend of generating a significant population (64.2%) of *trans* rotamers, with respect to the central torsion angle, similar to that observed for EG, was observed for ED simulated without 1−4 scaling. In addition, two types (G and G′) of *gauche* conformers were present, with an overall population of 35.8%.

Finally, the torsion angle distributions for two models of AE were examined to understand the specificity of the observed conformational behavior better. From the probability distribution of the NCCO dihedral angle for AE shown in Table 4, one can see a single intense peak corresponding to a 100% population of *gauche* rotamers. A very similar conformational pattern (not shown) was recorded for this model in the case of our scaling-free run. In contrast, the NCCO distribution for the AEtst model (also with no scaling) indicates the presence of *gauche* (20%) as well as *trans* (80%) conformers. Such a diversity of conformational patterns of AE leads one to the conclusion that dihedral angle distributions seem to be very sensitive to the chosen force fields. Therefore, in the lack of corresponding experimental data, they cannot be used as the only criterion in the search of the most appropriate model representations.

3.2.3. Comparison of Liquid-Phase Properties. The results of simulations performed with and without scaling of the 1−4 nonbonded interactions on the liquid-phase models of EG, ED, and AE are summarized in Table 5. One can clearly see that, for EG and ED, the conformation of the molecules, with respect to the central dihedral angle, changes from *gauche* to *trans* (a mixture of both types of rotamers are present in the case of ED) upon removal of scaling, whereas the conformation of AE remains consistently *gauche*. Experimentally, it has been found that *gauche* (G) is the most abundant conformation for EG[67,68] and AE[69] in the liquid state; this corresponds to results obtained in the present study when 1−4 scaling is used. For ED, the experimentally determined conformation (G+T or T)[2] is in excellent agreement with our observations from the scaling-free run. The populations of conformers of these models were calculated and are given in Table 4.

The experimental values for the heat of vaporization are also compared with the present calculated data in Table 5. One can see a similar trend of increasing magnitudes of ΔH_{vap} for EG and ED, comparing conventional and scaling-free results. For AE, the values obtained with and without scaling both seem to be slight underestimates, when compared with the corrected experimental result of 55.33 kJ/mol.[66] The scaling-free value of ΔH_{vap} for EG is ∼2 kJ/mol higher than the largest experimental estimate, whereas, for ED, the value obtained from the scaling-free simulation (40.01 kJ/mol) is more similar to the experimental value (44.98 kJ/mol)[62] than that obtained with conventional scaling factors.

A comparison of estimates of the self-diffusion coefficient (D) reveals a clear trend of decreasing magnitude in this quantity for the scaling-free simulation runs. For AE, D becomes approximately 2.5 times smaller with no 1−4 scaling (unfortunately, there is no experimental estimate available); for EG, the decrease is even more pronounced where the calculated value of 0.012×10^{-5} cm^2/s is 7.5 times lower than the experimental value (see Table 5). Somewhat surprisingly, the diffusion

TABLE 6: Thermodynamic Properties of Liquid Ethylene Glycol (EG), Ethylenediamine (ED), and 2-Aminoethanol (AE) Obtained from Simulations at 298 K

	EG	ED	AE	maximum error
$\langle U_a \rangle$ (kJ/mol)	6.02	11.78	9.62	
$\langle U_d \rangle$ (kJ/mol)	11.69	−7.17	2.64	
intramolecular energy (kJ/mol)				
$\langle U_Q \rangle$	90.71	148.67	81.11	0.20
$\langle U_{LJ} \rangle$	0.53	−0.31	0.87	0.05
intermolecular energy (kJ/mol)				
$\langle U_Q \rangle$	−48.80	−36.94	−48.16	0.57
$\langle U_{LJ} \rangle$	−12.24	−16.28	−13.65	0.03
$\langle \boldsymbol{U} \rangle$	**42.08**	**102.33**	**34.67**	**0.12**
pressure, P (atm)	703	−960	247	25

coefficient of ED decreases only slightly and achieves excellent agreement with experimental findings[70] with no scaling applied.

The results obtained for the AEtst model with no scaling (not shown in Table 5) can be summarized as it follows. This model gives rather poor performance for all quantities considered, in particular, the wrong conformation (see Section 3.2.2 for details) and a very low magnitude for the heat of vaporization (ΔH_{vap} = 37.88 kJ/mol). The self-diffusion coefficient for AEtst was determined to be $D = 0.35 \times 10^{-5}$ cm^2/s. The absence of an experimental result for D for AE and the fact that the only experimental ΔH_{vap} value available corresponds to the boiling temperature of AE makes it more difficult to justify completely a choice between the model representatives of this particular compound.

The present analysis indicates that the EG model simulated using the standard scaling scheme[43,45] provides superior results. It is also clear that all characteristics of the ED model obtained with scaling applied were dramatically improved in the scaling-free simulation run, making the latter model the obvious choice for further investigation. In the case of 2-aminoethanol, the AE model simulated with standard scaling was used in our further structural investigation and for the simulations of aqueous solutions.[37] A summary of the principal thermodynamic properties for the chosen models—in particular, Coulombic and LJ contributions to intramolecular and intermolecular energies, as well as the total configurational energies—are given in Table 6.

3.2.4. Structural Analysis of Pure Liquids. The structural analysis of pure liquid EG, ED, and AE was performed using both radial and spatial distribution functions (RDFs and SDFs, respectively). Despite of the fact that RDFs are functions of interparticle separation only and, therefore, ignore the orientation of the local frame, they are still widely used, because of their ability to provide some insights into the immediate environments of those atoms interacting strongly with other molecules or atoms. In strongly associated liquids, the most interesting and informative RDFs are usually those due to the atoms involved in hydrogen-bond formation. Nevertheless, in the present work, we have produced and examined RDFs and SDFs for all possible pairs of atoms including those for the C atoms. The latter functions often provide information about the possibile association between the hydrophobic components of molecules. As it was expected in the case of pure liquid EG, ED, and AE, no such phenomenon has been noted and corresponding RDFs and SDFs involving the C atom were not included in our structural analysis.

Commonly used hydrogen-bond definitions that appear in the literature are based on either energetic or geometric criteria.[9,31] It has also been previously shown that, in the case of alcohols (e.g., ethylene glycol), both energetic and geometric criteria lead to similar results in answering a question whether two molecules are hydrogen-bonded or not.[31] In the present work, we have adopted a geometric criterion that is based exclusively on the first peak of the appropriate RDFs. In particular, we assumed that a strong hydrogen bond exists if the positions of the first maxima fall in the ranges of 2.5−3.2 Å and 1.5−2.2 Å for RDFs between heavy atoms and between a heavy atom and the appropriate (amino or hydroxyl) hydrogen, respectively. Additional factors that are considered included the shape of the first peak (e.g., sharp, distinctive) and the depth of the corresponding first minima.

The RDFs between several site pairs for pure liquid EG, ED, and AE are shown in Figures 2, 3, and 4, respectively. The corresponding first coordination numbers (CN) were calculated as proposed in ref 71, and results are given in Table 7. The oxygen−oxygen (O−O) RDF for EG (Figure 2) shows a sharp first peak at 2.8 Å, which drops into the narrow minimum, followed by a broad second peak at ∼5.5 Å. The behavior exhibited by this function is somewhat reminiscent of the corresponding RDF of liquid methanol.[11] The O−H RDF has two peaks: one at 1.8 Å, due presumably to hydrogen bonding,

TABLE 7: Coordination Numbers Obtained for Pure Liquid Ethylene Glycol (EG), Ethylenediamine (ED), and 2-Aminoethanol (AE)[a]

atom pair[b]	coordination number, CN
EG	
O−O	3.0
O−H	1.0
ED	
N−N	3.6
N−H	1.0
AE	
O−O	1.0
N−N	1.7
N−O	2.2
O−H(N)	1.7
O−H(O)	0.5
N−H(N)	0.5
N−H(O)	0.5

[a] Intramolecular coordination is included in all results. [b] The first atom listed is the central atom.

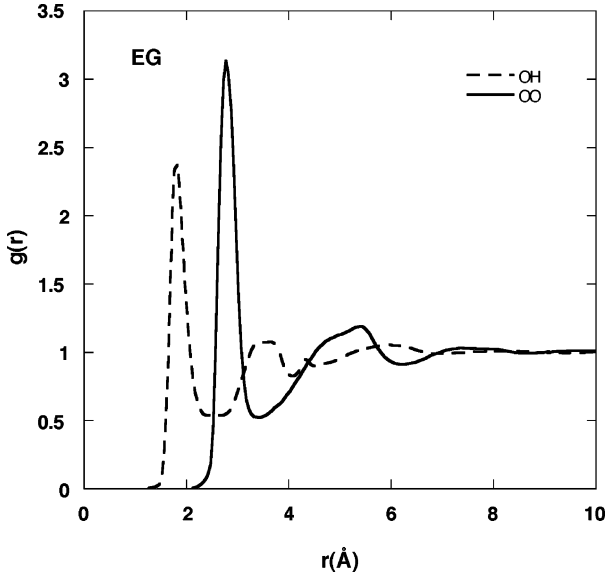

Figure 2. Radial distribution functions (RDFs) for pure liquid ethylene glycol at 298 K. The legend is as follows: (—) O−O RDFs and (- - -) O−H RDFs.

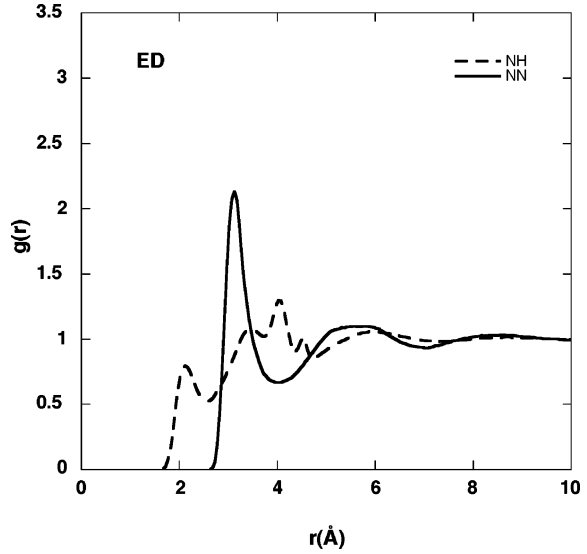

Figure 3. RDFs for pure liquid ethylenediamine (ED) at 298 K. The legend is as follows: (—) N−N RDFs and (- - -) N−H RDFs.

and a second, less well-defined maximum at 3.4 Å. These results for the RDFs of EG are in very good agreement with those of Saiz et al.[30] reported for two OPLS-based models of EG. Integration of the first peak of $g(r_{OH})$ gives a coordination number of 1.0, indicating that each O atom of EG accepts, on average, only one strong hydrogen bond, where this coordination can be due to intramolecular and intermolecular neighboring hydrogens. In addition, the coordination number from the first peak in the O−O RDF suggests the presence of three neighboring oxygens around each O atom. Clearly, one of these O atoms must be a strong hydrogen-bond acceptor and one a strong hydrogen-bond-donating neighbor, whereas the third atom does not seem to participate in a strong hydrogen bond. From the present RDF analysis, one can see that, although EG possesses a possible maximum of six hydrogen-bonding sites per molecule, two of which can participate in its intramolecular hydrogen bond, the constraint of hydrogen-bond balance (i.e., the requirement that the number of donors must equal the number of acceptors) dictates that two of the acceptor sites remain underutilizing, despite the apparent presence of two extra nearest-neighbor oxygens. The SDF analysis below will be used to provide additional insights into the nature of the near-neighbor coordination.

The RDFs of ED for N−N and N−H site pairs are shown in Figure 3. The N−N RDF exhibits a reasonably well-defined but small first peak at 3.1 Å, followed by a shallow minimum at 4 Å and a broad second peak at ∼5.5 Å. The N−H RDF has a small first peak at 2.1 Å that is due to relatively weaker (in comparison to EG) hydrogen-bonded neighbors, as well as a quite complicated set of peaks at larger separations, corresponding to a secondary structure; one can distinguish a maximum at 4.0 Å located between two shoulders at 3.5 and 4.4 Å. Unfortunately, neither theoretical nor experimental RDFs of ED were found in the available literature for comparison.

Analysis of the coordination numbers for liquid ED requires that we recall that ∼65% of the molecules in our model system adopt a *trans* conformation and, hence, only one-third of all rotamers may possess an intramolecular hydrogen bond. Integration of the first peaks in $g(r_{NH})$ and $g(r_{NN})$ yields coordination numbers of 1.0 and 3.6, respectively (see Table 7). One can reasonably assume that one-third of the H atoms that are hydrogen-bonded to a N atom are from within the same molecule. Taking into account that ED has four hydrogen-bond donor sites and two hydrogen-bond acceptor sites per molecule, one can suggest that each molecule makes, on average, four relatively strong hydrogen bonds while two of the donating sites do not seem to participate in strong hydrogen bonding. As complementary evidence for this, the N−N coordination number indicates the presence of at least two non-hydrogen-bonding (or weakly hydrogen-bonding) nitrogens located in the first coordination shell of the ED molecule.

Seven selected RDFs between O, N, and their associated H atoms for pure AE are presented in Figure 4. The first distinctive peak in the N−O RDF (see Figure 4a) can be identified as one due to the hydrogen-bonded O atom and N atom at an interatomic distance of 2.9 Å; a small shoulder at 3.7 Å is an intramolecular feature corresponding to the presence of a small amount of *trans* conformer. The O−O and N−N functions are compared in Figure 4b. The O−O RDF exhibits a well-defined, sharp peak at 2.7 Å that drops into the deep minimum, followed by a broad peak due to second-nearest neighbors. In contrast, the N−N RDF has a smaller and broader first peak at 3.1 Å, followed by a similarly broad second maximum (at ∼5.6 Å). Four RDFs of the O−H or N−H type (with amino or hydroxyl hydrogens) are shown in Figure 4c and 4d. Both O−H(O) and N−H(O) RDFs have large and well-defined first peaks at 1.8 and 1.9 Å, respectively, indicating the presence of strong hydrogen bonding between the corresponding sites, where contributions due to intramolecular and intermolecular nearest neighbors overlap. In the O−H(O) function, the second peak is less well-defined, whereas the second peak in N−H(O) has a distinct maximum at 3.7 Å. The O−H(N) has two broader peaks at 2.3 Å, likely due to the overlapped contributions from a strong hydrogen-bonded neighbor and a weaker hydrogen-bonded neighbor, and a peak at 3.2 Å whose identity is not resolvable from the RDF. The less-pronounced (i.e., appearing more as a shoulder) hydrogen-bonded peak observed at 2.1 Å in the N−H(N) RDF suggests that the N donor sites have a tendency to form rather few hydrogen bonds with other N atoms. Finally, note that the four O−H and N−H RDFs are all in good qualitative agreement with the results reported by Alejandre et al.;[35] some exceptions for O−H(N) can be explained by the difference in the model potentials used.

The coordination numbers of AE listed in Table 7 reveal some interesting trends. For instance, the like−like atomic coordination number for both N and O atoms (1.0 and 1.7) is smaller than the value of 2.2 from $g(r_{NO})$, which confirms a preference for unlike-atom coordination. In addition, the total coordination around N and O atoms that is due to hydroxyl and amino hydrogens is 2.2, which is equal to the value from $g(r_{NO})$, indicating that all O−N site pairs seem to be strongly hydrogen-bonded. Analysis of the total coordination numbers also suggests that the AE molecule has, on average, seven nearest neighbors, among which three seem to be donors whereas three other are acceptors of strong hydrogen bonds. The remaining one neighbor is presumably weakly hydrogen-bonded to the N atom, making its total coordination number 4. In addition, coordination numbers for O−H(N) and N−H(O), and the corresponding RDFs, clearly indicate the preference for N−H···O versus O−H···N hydrogen bonds, which leads to the conclusion that, in the liquid phase, AE should have a tendency to adopt the gGt conformation. This result can be confirmed by previous experimental[69] and theoretical[27] findings.

To get more detailed insights into the three-dimensional local structure around EG, ED, and AE in their pure liquids, SDFs[72] were calculated and visualized (see Figures 5−8). For the sake

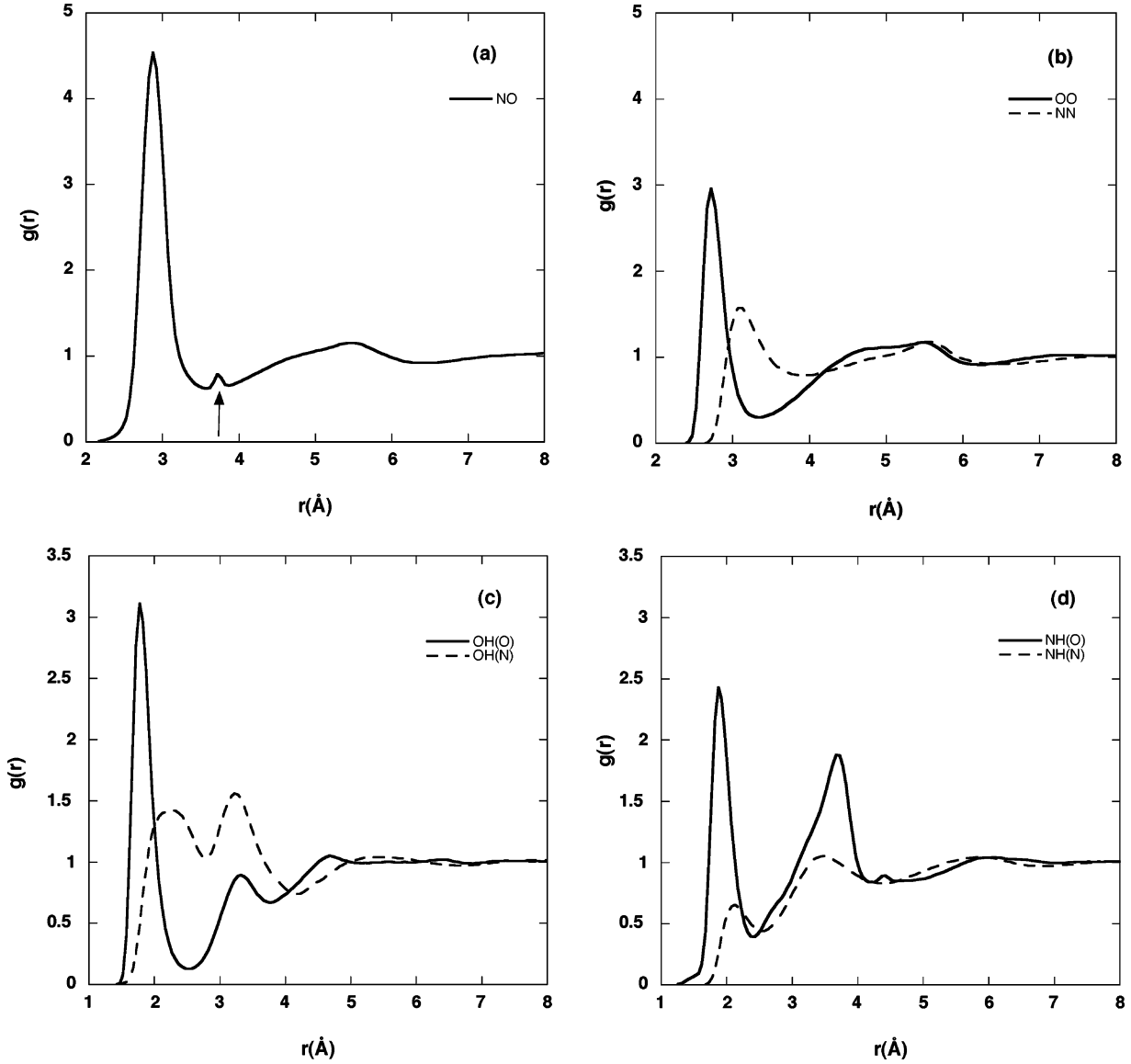

Figure 4. RDFs for pure liquid 2-aminoethanol at 298 K: (a) N−O (the arrow indicates an intramolecular feature) and (b) O−O and N−N RDFs (the latter functions are represented by solid and dashed lines, respectively). Panels (c) and (d), respectively, show O−H and N−H site−site RDFs. Solid lines correspond to the functions involving hydroxyl hydrogen, whereas dashed lines represent functions involving amino hydrogen.

of clarity only the fragment of the central molecule defining the local frame for each compound is represented in Figures 5−8. This fragment is always composed of the appropriate functional group (i.e., hydroxyl for EG, amino for ED, and both for AE) and its attached C atom.

In panels a and b in Figure 5, the O−O SDFs for EG are shown for thresholds 3.0 and 1.8 times greater than the bulk density, respectively. In Figure 5a, one can see four different features that are due to nearest neighbors. Two of them (located below and above the hydroxyl group) are the principal features corresponding to donors and acceptors of strong intermolecular hydrogen bonds. The wide ring around the C atom is due to the intramolecular O atom (the second O atom on the EG molecule) when the molecule is in the *gauche* conformation, with respect to the central dihedral angle, and, at the same time, performs rotation around the O−C bond (i.e., rotation with respect to the HOCC dihedral angle). The second small ring, which is not well-defined at this threshold, also indicates the same type of rotation of the second O atom when the central molecule adopts the *trans* conformation, with respect to the OCCO dihedral angle.

At the lower isosurface threshold (shown in Figure 5b), the SDF becomes more complex. The red distant features correspond to the secondary structure. These are the round-shaped features behind the principal hydrogen-bond acceptor, the group of features around the central ring (these are nearest neighbors, with respect to the second intramolecular oxygen), and the feature above the small ring due to first neighbors to the oxygen in the *trans* position. It is especially interesting to note the appearance of a ridge on the hydrogen-bond-donating feature, which becomes larger and develops two "wings" on both sides extending upward toward the cap, because of the hydrogen-bond acceptor. It is likely that the ridge indicates the presence of a rather weak hydrogen-bond donor, which is trying to occupy a second accepting site on the central O atom. As has been shown previously, the "wings" that develop at larger separations on the edge of the principal hydrogen-bond donor feature are evidence of the presence of possible bifurcated hydrogen-bond arrangements.[15]

The O−H SDFs for EG (Figure 6) provide additional confirmation of the formation of a structural picture. In Figure 6a, one can see that, at a threshold of 5.0, only strong hydrogen-

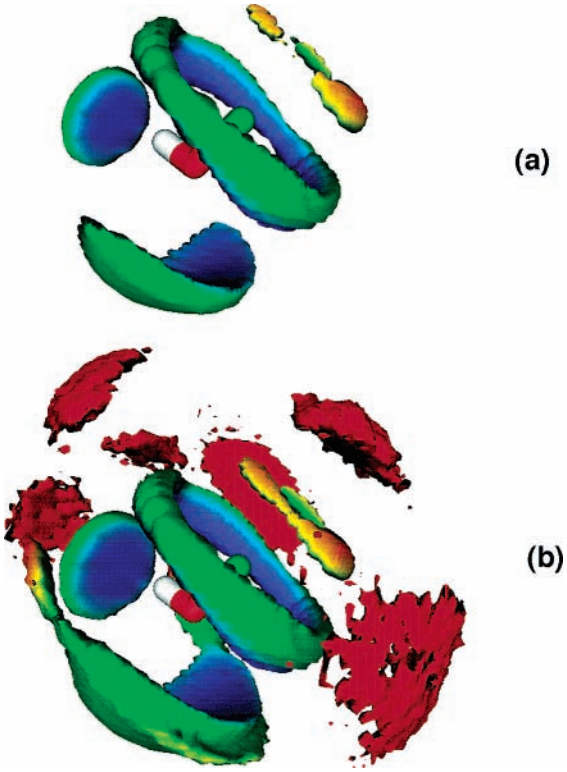

Figure 5. Oxygen−oxygen spatial distribution functions for pure liquid ethylene glycol at 298 K. Isosurface thresholds of (a) 3.0 and (b) 1.8 are shown. The surfaces are colored based on separation, from 2.5 Å (dark blue) to 4.0 Å and larger (red).

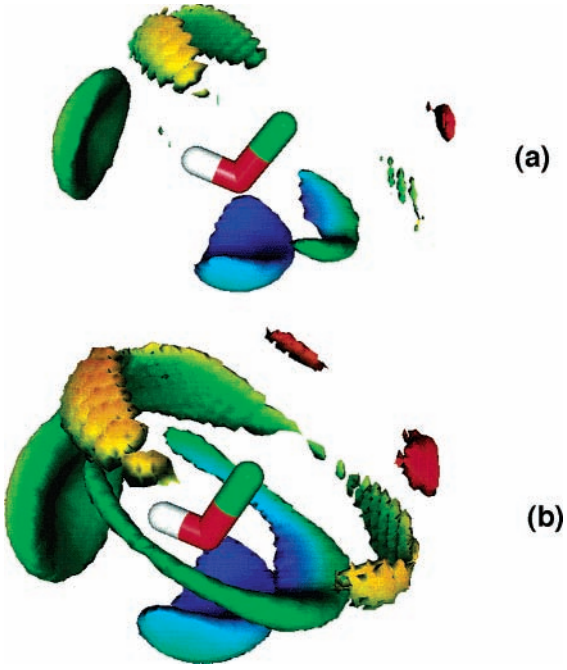

Figure 6. Oxygen−hydrogen SDFs for pure liquid ethylene glycol at 298 K. Isosurface thresholds of (a) 5.0 and (b) 2.5 are shown. The surfaces are colored based on separation, from 1.5 Å (dark blue) to 4.5 Å and larger (red).

bonded features around the central molecule survive at this relatively high threshold, in particular, the feature that is due to the H atom attached to the accepting O atom (in front of the H atom on the hydroxyl group) and the H atom directly hydrogen-bonded to the central O atom. The four other features that are apparent in Figure 6a are due to intramolecular

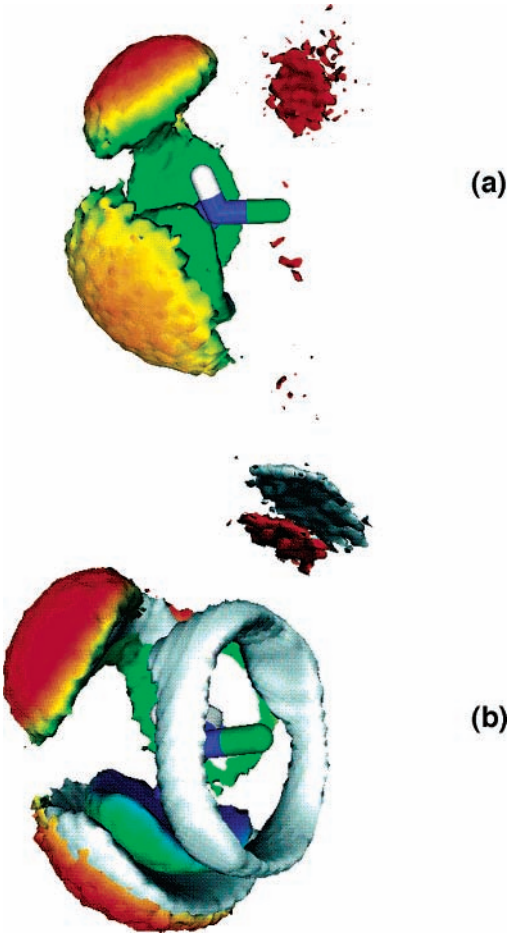

Figure 7. SDFs for pure liquid ethylenediamine at 298 K: (a) N−H at a threshold of 1.5 and (b) N−H at a threshold of 1.6 overlayed with N−N at a threshold of 2.3 (light shading). The isosurfaces are colored based on separation from 2.0 (dark blue) to 4.5 Å and larger (red).

hydrogens (analogous to the O−O SDF) and are not fully resolved at this threshold, although they become more pronounced at a threshold of 2.5 (see Figure 6b) and can be identified as follows. Two small, more-distant (red) features are created, because of intramolecular H atoms directly attached to the O atom in the *trans* position, as well as those hydrogen-bonded to it. The large ring around the C atom is due to H atoms associated with the intramolecular O atom; the H atom covalently bonded to this O atom contributes to the upper portion of the ring, whereas the hydrogen-bonded intermolecular H atom is responsible for the presence of its lower part. The identification of these features can be additionally confirmed by overlapping the O and H SDFs (from Figures 5 and 6, respectively). The "U-shaped" feature next to the central O atom consists of a smeared cap and two long "wings" broadened at the ends. Its lower part (the cap) is also due to the H atom covalently bonded to the intramolecular O atom when an EG molecule adopts an inverse conformation (i.e., tG′g versus tGg′) and the "wings" are another indication of a weak hydrogen-bond donor. Although the corresponding weak hydrogen-bond acceptor feature could not be specifically identified, it becomes apparent that a EG molecule has a tendency to participate in two weak (possibly birfurcated) hydrogen bonds, in addition to four strong ones, which is in agreement with the results of the present radial and CN analysis.

The local structure around ED has been explored through the N−H and N−N SDFs (see Figure 7). The N−H SDF at a threshold of 1.5 shown in Figure 7a exhibits several features

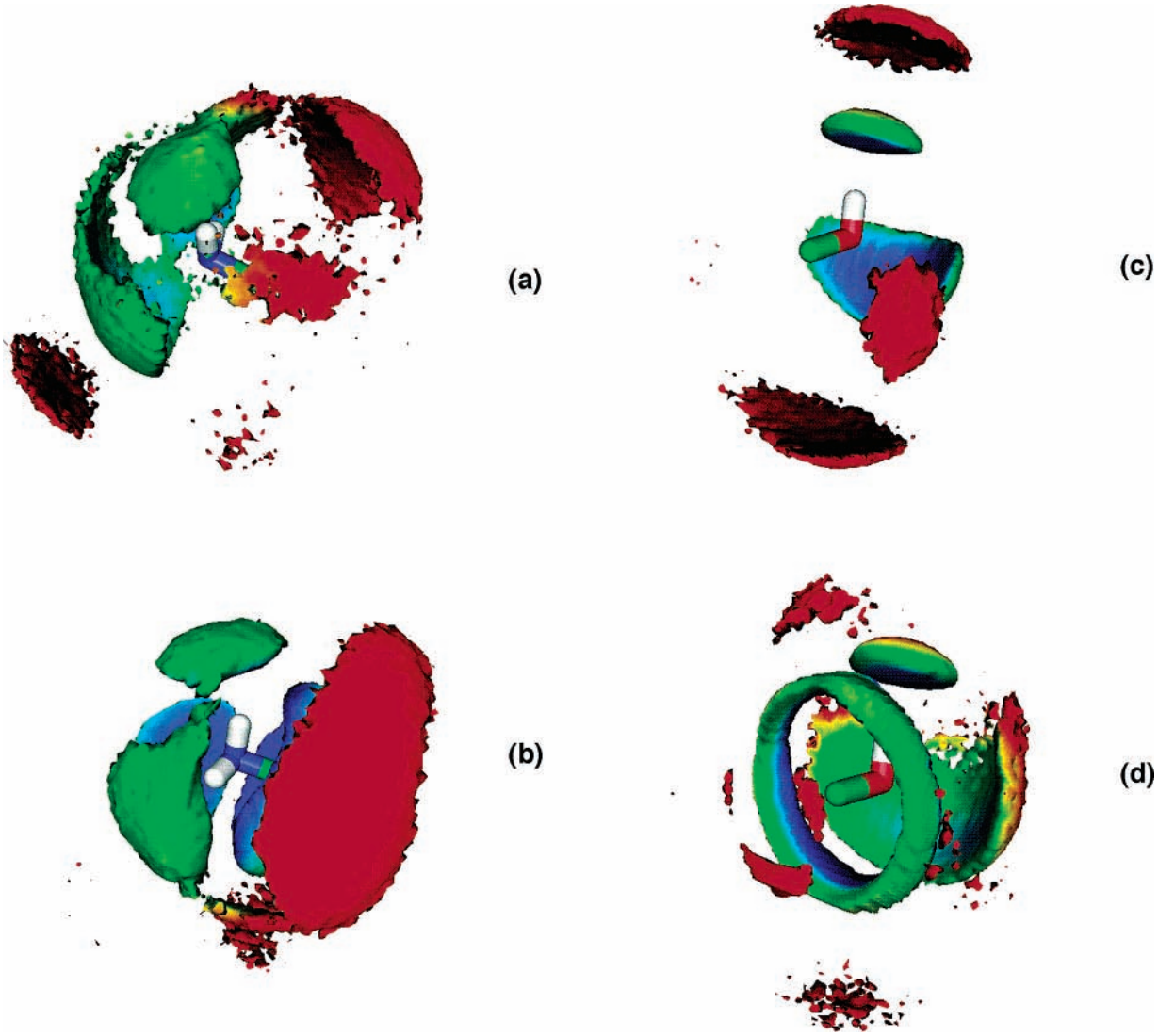

Figure 8. SDFs for pure liquid 2-aminoethanol at 298 K: (a) N−N (at a threshold of 1.9), (b) N−O (at a threshold of 1.9), (c) O−O (at a threshold of 2.5), and (d) O−N (at a threshold of 2.3) SDFs. The isosurfaces are colored based on separation, as in Figure 5.

including those due to strong hydrogen bonds. The single feature below the nitrogen corresponds to a single hydrogen-bond-donating neighbor, whereas each of the two caps connected by a wide "bridge" and located above the amine hydrogens combine to account for a second strong and a third weakly hydrogen-bonded nearest neighbor.[15] The large cap below the single hydrogen-bond-donating feature is due to the second H atom of the amino group donating the hydrogen bond to the central N atom. The small (red) distant feature seems to be a rather weakly hydrogen-bonded nearest neighbor, which unexpectedly approaches the amino group from "above". The presence of the large (∼2/3) population of *trans* conformations in pure ED make such arrangements possible. Interestingly, no features associated with intramolecular hydrogen density (i.e., from the second amino group in the *trans* position) were noted. This can be interpreted as being a manifestation of the greater flexibility of the ED model; we recall that no scaling was applied for 1−4 nonbonded interactions in ED.

From Figure 7b, where the N−H SDF is superimposed with the corresponding N−N SDF, the local structural arrangement in liquid ED is further clarified. First, one can see the appearance of the large ring, because of internal rotation of the *gauche* N atom (pure ED has 36% *gauche* rotamers) and the nitrogen density above the feature due to the weakly hydrogen-bonded hydrogen. The principal hydrogen-bonded features become multilayered (doubly for the hydrogen-bond-accepting features and triply for the hydrogen-bond-donating features), because of the presence of both H and N atoms in the strongly associated amino groups. One can again conclude that, within liquid ED, somewhat similar to the situation for EG, the N atom of ED participates in two strong and two weak hydrogen bonds.

The SDFs for the two functional groups of AE (see Figure 8) demonstrate a structure somewhat similar to that observed for their counterparts in EG and ED. The N−N and N−O SDFs are presented at a threshold of 1.9 in Figures 8a (as the "side" view of the amino group) and 8b (shown from the "front" of the amino group), respectively. In both SDFs, well-defined features that are due to hydrogen-bonded nearest neighbors are clearly evident. The N−N structure in AE has some similarities to that of ED (i.e., principal features) but there are noticeable differences, presumably due to the fact that the N atom in AE is trying to accommodate its 4-coordination, where one of these neighbors is a weakly bonded N atom. In Figure 8a, one can see a feature that bridges the two caps centered over the amine H atoms and has a tendency to connect to the more-distant secondary feature. This large extended cap, appearing red at a separation of ∼4.0 Å from the central N atom, corresponds to a secondary N atom; it can be identified as a nearest hydrogen-

bonded neighbor for the intramolecular O atom in *gauche* position. For liquid methylamine,[15] it was shown that the extension of principal hydrogen-bonding features to larger separations indicates that neighboring molecules located over the hydrogen-bonding sites form weak (backside or bifurcated) hydrogen-bond arrangements. The presence of two extended features (red shading) in Figure 8a leads to the claim that, in liquid AE, nitrogen, which has four nearest neighbors on average, participates in three strong hydrogen bonds, as well as one much weaker hydrogen bond. In addition, interesting phenomena can be noted from the local oxygen density around the N atom shown in Figure 8b. A rim that is apparent on at least one of the principal hydrogen-bond-accepting features may serve as an indication of a transient structure that results from the rotation of the amino group, which allows both amino H atoms to participate in the formation of an intermolecular hydrogen bond with a neighboring O atom. The broad ring that is typical for this intramolecular O atom can also be seen in Figure 8b; it is somewhat obscured by a more-distant elongated secondary feature, which can be again identified as intermolecular oxygen density nearest and hydrogen-bonded to the O atom of the intramolecular ring.

The hydrogen-bonding pattern observed in O−O and O−N SDFs (see Figures 8c and 8d, respectively) has both familiar and unfamiliar aspects. The highly localized arrangement of the two hydrogen-bonding caps (particularly, the donor feature), as well as the presence of a secondary feature recorded above the hydroxyl H atom in the O−O SDF (see Figure 8c), sharply contrasts that observed in the O−N SDF. In Figure 8d, the hydrogen-bond-donating feature is represented by the extended slightly dipolar cap and no secondary structure that is associated with the hydrogen-bond-accepting feature is observed. Somewhat similar secondary structural arrangements located around central C atom can be observed on both O−O and O−N SDFs. They are primarily associated with the intramolecular N atom in the *gauche* position (represented by the large ring in Figure 8d). In addition, the presence of a very small amount of atomic density due to the intramolecular N atom in *trans* position can be recognized in the three small features outlining a second ring in Figure 8d. Together, the results displayed in Figure 8 indicate that both the N and O atoms of AE participate in three strong hydrogen bonds. It was possible to identify the location of one (as it follows from CN analysis) remaining weakly hydrogen-bonded nearest-neighbor atom. However, note that such features can be expected to be rather sensitive to the quality of the model potential used for this particular compound.

4. Conclusions

In this paper, we reported results of a computer simulation study of the local liquid state structure of three representatives of 1,2-disubstituted ethanes, namely, ethylene glycol (EG), ethylenediamine (ED), and 2-aminoethanol (AE). Classical molecular dynamics (MD) simulations were performed, combined with several methods of analysis, including a relatively new technique that utilized spatial distribution functions (SDFs). The purpose of this investigation was to clarify the conformational picture and to obtain a detailed description of the hydrogen-bonding patterns and local structure in these liquid systems.

Twelve molecular models were constructed to test different potentials (i.e., force fields) and molecular representations. Gas-phase (isolated single molecule) simulations were performed, and simulated geometries and conformations were compared with the most reliable experimental estimates. Consequently, the five most successful models were chosen; the molecular descriptions of each of these models included the OPLS-based parametrization for alcohols and amines.[6,40] Liquid-phase simulations for EG, ED, and AE were then performed. The influences of inclusion and of the values of scaling coefficients for the Lennard-Jones (LJ) and Coulombic contributions to 1−4 nonbonded interactions were examined. The experimental heats of vaporization and self-diffusion coefficients were used as criteria for the final selection of molecular models. Note that there had been no previous simulation results reported in the literature for the heat of vaporization and self-diffusion coefficient for pure liquid AE. It was shown that, for EG and AE, the best agreement of simulated properties with experimental estimates is achieved when scaling factors of 0.125 and 0.833 were used for the LJ and Coulombic terms, respectively; no scaling was necessary in the case of ED. For all three liquids, the chosen models were shown to provide good agreement with the experiment where data were available.

An important part of our structural analysis for liquid-phase EG, ED, and AE was the determination of dihedral angle distributions for the central (XCCY) dihedral angles. For these molecules, the value of the central torsional angle is critical to the presence of an intramolecular hydrogen bond, which significantly impacts the local structure. The relative populations revealed a clear preference for the *gauche* conformers for liquid EG and AE, whereas ED seems to be primarily in the *trans* form. In the absence of quantitative experimental data, these results are in very good qualitative agreement with available experimental estimates.

The investigation of the local structure around the EG, ED, and AE molecules in their pure liquids included analysis of radial distribution functions (RDFs) and coordination numbers, as well as production and interpretation of SDFs. The radial analysis, in conjunction with calculated numbers of nearest neighbors around the O and N atoms of the main functional groups, provided some structural insights into the hydrogen-bonding pattern within the pure systems. The number of strongly hydrogen-bonded neighboring groups (among all recorded nearest neighbors) was determined, and then their relative positions, with respect to the reference (central) atom, have been located by means of SDFs. Through this analysis, it was found that, in EG and ED, both O and N atoms have a tendency to make, on average, two strong hydrogen bonds, apparently leaving one acceptor and one donor site, respectively, underutilized. Such behavior can be interpreted as a direct consequence of the requirements imposed by hydrogen-bond balance (i.e., that the total number of acceptors must equal the total number of donors). In addition, the O atom of EG exhibited one weakly hydrogen-bonded neighbor, and the N atom of ED two weakly hydrogen-bonded neighbors, for which much of the corresponding local densities were successfully identified during the spatial analysis. These weakly hydrogen-bonded neighbors appear often in holes or otherwise unoccupied positions in the local structure. The structural picture for the functional groups of AE seems somewhat similar to that observed in EG and ED. However, both amino and hydroxyl groups are strongly hydrogen-bonded to three neighbors, which is now allowed by hydrogen-bond balance. An additional weakly bound nearest neighbor of the N atom of AE was not clearly identifiable on the corresponding atomic density maps. The possibility of three- and four-membered arrangements around a central hydrogen-bonding group leads one to the conclusion that, in liquid EG, ED, and AE, the generalized hydrogen-bonding pattern can be described as a three-dimensional, branched network. For all three mol-

ecules, the presence (or absence) of an internal hydrogen bond was observed to impact their hydrogen-bonding structure significantly. The present SDF analysis has allowed us to examine the rather complex nature of these networks and to identify the elements directly involved in its formation.

On the basis of previously obtained results for pure liquid methanol,[11] methylamine,[15] and *tert*-butyl alcohol,[73] one might expect that the representatives of 1,2-disubstituted ethanes investigated in this work would demonstrate a reasonably high degree of cooperativity, that is, where the structure around one hydrogen-bonding group is significantly perturbed by the presence or nature of a neighboring functional group within the same molecule (for example, to maintain local hydrogen-bond balance). Little tendency toward this type of behavior was observed during comparison of the major features noted in the local structures around the O and N atoms, respectively, of EG and ED with those registered in liquid AE. Yet, it was also noted in the case of AE, where both hydroxyl and amino groups are present, that the hydrogen-bond arrangements around a particular group can be strongly influenced by the identity of the coordinating neighbor. Furthermore, it was determined that the local structure around the functional groups of these 1,2-disubstituted ethanes did differ in significant ways from that observed in methanol and methylamine. Thus, it was confirmed that the constraints imposed by the molecular geometry (bonding), as well as those associated with the most-abundant liquid-phase conformations (i.e., the formation of internal hydrogen bonds), have critically important roles in determining the specific nature of the local structure in pure liquid EG, ED, and AE.

Acknowledgment. A.G. thanks Dr. A. Laaksonen and Dr. A. Lyubartsev for providing assistance in the utilization of M.DynaMix simulation package. This work has been supported by the Natural Science and Engineering Research Council of Canada (NSERC).

References and Notes

(1) Radom, L.; Lathan, W. A.; Hehre, W. J.; Pople, J. A. *J. Am. Chem. Soc*. **1973**, *95*, 693.
(2) Batista de Carvalho, L. A. E.; Lourenco, L. E.; Marques, M. P. M. *J. Mol. Struct. (THEOCHEM)* **1999**, *482*−*483*, 639.
(3) *Kirk*−*Othmer Encyclopedia of Chemical Technology*, 3rd ed.; Wiley: New York, 1978; Vol. 1.
(4) Luo, R.-Sh.; Jonas, J. *J. Raman Spectrosc*. **2001**, *32*, 975.
(5) Teppen, B. J.; Cao, M.; Frey, R. F.; van Alsenoy, Ch.; Miller, D. M.; Schafer, L. *J. Mol. Struct. (THEOCHEM)* **1994**, *314*, 169.
(6) Jorgensen, W. L. *J. Phys. Chem*. **1986**, *90*, 1276.
(7) Narten, A. H.; Habenschuss, A. *J. Chem. Phys*. **1984**, *80*, 3387.
(8) Hamilton, W. C.; Ibers, J. A. *Hydrogen Bonding in Solids: Methods of Molecular Structure Determination*; W. A. Benjamin: New York, 1968.
(9) Haughney, M.; Ferrario, M.; McDonald, I. R. *J. Phys. Chem*. **1987**, *91*, 4934.
(10) Jorgensen, W. L. *J. Am. Chem. Soc*. **1981**, *103*, 341.
(11) Svishchev, I. M.; Kusalik, P. G. *J. Chem. Phys*. **1994**, *100*, 5165.
(12) Laaksonen, A.; Kusalik, P. G.; Svishchev, I. M. *J. Phys. Chem. A* **1997**, *101*, 5910.
(13) Jorgensen, W. L.; Madura, J. D. *J. Am. Chem. Soc*. **1983**, *105*, 1407.
(14) Soper, A. K.; Finney, J. L. *Phys. Rev. Lett.* **1993**, *71*, 4346.
(15) Kusalik, P. G.; Bergman, D.; Laaksonen, A. *J. Chem. Phys*. **2000**, *113*, 1.
(16) Hamada, Y.; Tsuboi, M.; Nakata, M.; Tasumi, M. *J. Mol. Spectrosc*. **1984**, *106*, 164.
(17) Rodnikova, M. N.; Isaev, A. N.; Zasypkin, S. A. *Koord. Khim.* **1991**, *17*, 1467. (Journal written in Russian.)
(18) Chang, Y.-P.; Su, T.-M.; Li, T.-W.; Chao, I. *J. Phys. Chem*. **1997**, *101*, 6107.
(19) Kudoh, S.; Takayanagi, M.; Nakata, M.; Ishibashi, T.; Tasumi, M. *J. Mol. Struct. (THEOCHEM)* **1999**, *479*, 41.
(20) Bultinck, P.; Goeminne, A.; Vondel, D. V. *J. Mol. Struct. (THEOCHEM)* **1995**, *339*, 1.
(21) Yeh, T.-S.; Chang, Y.-P.; Su, T. M. *J. Phys. Chem*. **1994**, *98*, 8921.
(22) Cramer, C. J.; Truhlar, D. G. *J. Am. Chem. Soc*. **1994**, *116*, 3892.
(23) Kreuger, P. J.; Mettee, H. D. *Can. J. Chem*. **1965**, *43*, 2970.
(24) Penn, R. E.; Curl, R. F. *J. Chem. Phys*. **1971**, *55*, 651.
(25) Kelterer, A.-M.; Ramek, M. *J. Mol. Struct. (THEOCHEM)* **1991**, *232*, 189.
(26) Buemi, G. *Int. J. Quantum Chem*. **1996**, *59*, 227.
(27) Vorobyov, I.; Yappert, M. C.; DuPre, D. B. *J. Phys. Chem*. **2002**, *106*, 668.
(28) Nagy, P. I.; Dunn, W. J., III; Alagona, G.; Ghio, C. *J. Am. Chem. Soc*. **1991**, *113*, 6719.
(29) Burgess, A. W.; Shipman, L. L.; Nemenoff, R. A.; Scheraga, H. A. *J. Am. Chem. Soc*. **1976**, *98*, 23.
(30) Saiz, L.; Padro, J. A.; Guardia, E. *J. Chem. Phys*. **2001**, *114*, 3187.
(31) Padro, J. A.; Saiz, L.; Guardia, E. *J. Mol. Struct. (THEOCHEM)* **1997**, *416*, 243.
(32) Widmalm, G.; Pastor, R. W. *J. Chem. Soc., Faraday Trans*. **1992**, *88*, 1747.
(33) Hayashi, H.; Tanaka, H.; Nakanishi, K. *Fluid Phase Equilib*. **1995**, *104*, 421.
(34) Button, J. K.; Gubbins, K. A.; Tanaka, H.; Nakanishi, K. *Fluid Phase Equilib.* **1996**, *116*, 320.
(35) Alejandre, J.; Rivera, J. L.; Mora, M. A.; de la Garza, V. *J. Phys. Chem. B* **2000**, *104*, 1332.
(36) Chandrasekhar, N.; Krebs, P. *J. Chem. Phys*. **2000**, *112*, 5910.
(37) Gubskaya, A. V.; Kusalik, P. G. *J. Phys. Chem. A* **2004**, *108*, 7165.
(38) Jorgensen, W. L.; Madura, J. D.; Swenson, C. J. *J. Am. Chem. Soc*. **1984**, *106*, 6638.
(39) Ryckaert, J.-P.; Ciccotti, G.; Berendsen, H. J. C. *J. Comput. Phys*. **1977**, *23*, 327.
(40) Rizzo, C. R.; Jorgensen, W. L. *J. Am. Chem. Soc*. **1999**, *121*, 4827.
(41) Jorgensen, W. L.; Maxwell, D. S.; Tirado-Rives, J. *J. Am. Chem. Soc*. **1996**, *118*, 11225.
(42) (a) Allinger, N. L.; Yuh, Y. H.; Lii, J.-H. *J. Am. Chem. Soc*. **1989**, *111*, 8551. (b) Lii, J.-H.; Allinger, N. L. *J. Am. Chem. Soc*. **1989**, *111*, 8566; (c) Lii, J.-H.; Allinger, N. L. *J. Am. Chem. Soc*. **1989**, *111*, 8576.
(43) Cornell, W. D.; Cieplak, P.; Bayly, Ch. I.; Kollman, P. A. *J. Am. Chem. Soc*. **1993**, *115*, 9620.
(44) DeBolt, S. E.; Kollman, P. A. *J. Am. Chem. Soc*. **1995**, *117*, 5316.
(45) Tirado-Rives, J.; Jorgensen, W. L. *J. Am. Chem. Soc*. **1990**, *112*, 2773.
(46) Allen, M. P.; Tildesley, D. J. *Computer Simulation of Liquids*; Clarendon Press: Oxford, 1987.
(47) Lyubartsev, A. P.; Laaksonen, A. *Comput. Phys. Commun*. **2000**, *128*, 565.
(48) Ivanova, E. F.; Kiiko, S. M. *Visn. Khark. Univ.* **1993**, *378*, 92. (Journal written in Russian.)
(49) Aminabhavi, T. M.; Gopalakrishna, B. *J. Chem. Eng. Data*. **1995**, *40*, 856.
(50) Maham, Y.; Teng, T. T.; Hepler, L. G.; Mather, A. E. *J. Solution Chem*. **1994**, *23*, 195.
(51) Nosé, S. *J. Chem. Phys*. **1984**, *81*, 511.
(52) Hoover, W. G. *Phys. Rev. A* **1985**, *31*, 1695.
(53) Frisch, M. J.; Trucks, G. W.; Schlegel, H. B.; Scuseria, G. E.; Robb, M. A.; Cheeseman, J. R.; Zakrzewski, V. G.; Montgomery, J. A., Jr.; Stratmann, R. E.; Burant, J. C.; Dapprich, S.; Millam, J. M.; Daniels, A. D.; Kudin, K. N.; Strain, M. C.; Farkas, O.; Tomasi, J.; Barone, V.; Cossi, M.; Cammi, R.; Mennucci, B.; Pomelli, C.; Adamo, C.; Clifford, S.; Ochterski, J.; Petersson, G. A.; Ayala, P. Y.; Cui, Q.; Morokuma, K.; Malick, D. K.; Rabuck, A. D.; Raghavachari, K.; Foresman, J. B.; Cioslowski, J.; Ortiz, J. V.; Stefanov, B. B.; Liu, G.; Liashenko, A.; Piskorz, P.; Komaromi, I.; Gomperts, R.; Martin, R. L.; Fox, D. J.; Keith, T.; Al-Laham, M. A.; Peng, C. Y.; Nanayakkara, A.; Gonzalez, C.; Challacombe, M.; Gill, P. M. W.; Johnson, B. G.; Chen, W.; Wong, M. W.; Andres, J. L.; Head-Gordon, M.; Replogle, E. S.; Pople, J. A. *Gaussian 98*, revision A.11.2; Gaussian, Inc.: Pittsburgh, PA, 1998.
(54) http://www.csc.fi/gopenmol/.
(55) Caldwell, J. W.; Kollman, P. A. *J. Phys. Chem.* **1995**, *99*, 6208.
(56) Brooks, B. R.; Bruccoleri, R. E.; Olafson, B. D.; States, D. J.; Swaminathan, S. Karplus, M. *J. Comput. Chem*. **1983**, *4*, 187.
(57) MacKerell, A. D., Jr.; Wiorkiewicz-Kuczera, J.; Karplus, M. *J. Am. Chem. Soc*. **1995**, *117*, 11946.
(58) Marstokk, K.-M.; Mollendal, H. *J. Mol. Struct. (THEOCHEM)* **1978**, *49*, 221.
(59) Caminati, W.; Corbelli, G.; *J. Mol. Spectrosc.* **1981**, *90*, 572.
(60) Buckley, P.; Giguere, P. A. *Can. J. Chem*. **1967**, *45*, 397.
(61) Gallaugher, A. F.; Hibbert, H. *J. Am. Chem. Soc*. **1937**, *59*, 2521.
(62) Weast, R. C., Ed. *CRC Handbook of Chemistry and Physics*, 64th ed.; CRC Press: West Palm Beach, FL, 1983.

(63) Knauth, P.; Subbuh, R. *Bull. Soc. Chim. Fr*. **1988**, 834.
(64) Knauth, P.; Subbuh, R. *J. Chem. Thermodyn*. **1989**, *21*, 203.
(65) Knauth, P.; Subbuh, R. *Struct. Chem*. **1990**, *1*, 43.
(66) Majer, V.; Svoboda, V. *Enthalpies of Vaporization of Organic Compounds*; Blackwell Scientific Publications: Oxford, 1985.
(67) Crupi, V.; Jannelli, M. P.; Magazu, S.; Maisano, G.; Majolino, D.; Migliardo, P.; Sirna, D. *Mol. Phys*. **1995**, *84*, 645.
(68) Crupi, V.; Maisano, G.; Majolino, D.; Migliardo, P.; Venuti, V. *J. Phys. Chem. A* **2000**, *104*, 3933.
(69) Silva, C. F. P.; Duarte, M. L. T. S.; Fausto, R. *J. Mol. Struct. (THEOCHEM)* **1999**, *482*−*483*, 591.
(70) Samigullin, F. M.; Rodnikova, M. N.; Val'kovskaya, T. M. *Zh. Neorg. Khim*. **1997**, *42*, 1049. (Journal written in Russian.)
(71) Ben-Naim, A. *Water and Aqueous Solutions. Introduction to a Molecular Theory*; Plenum Press: New York, 1974.
(72) Svishchev, I. M.; Kusalik, P. G. *J. Chem. Phys*. **1993**, *99*, 3049.
(73) Kusalik, P. G.; Lyubartsev, A. P.; Bergman, D. L.; Laaksonen, A. *J. Phys. Chem. B* **2000**, *104*, 9526.